Elastic properties and anisotropic effects on waves propagation of zinc-ferrite spinel systems as a function of pressure

Óscar A. Restrepo, Óscar Arnache, J. Restrepo, Charlotte Becquart

Elastic properties and anisotropic effects on waves propagation of zinc-ferrite spinel systems as a function of pressure

Óscar A. Restrepo[a,b], Óscar Arnache[c], J. Restrepo[a] and Charlotte S. Becquart[d]

[a] Grupo de Magnetismo y Simulación G+, Instituto de Física, Universidad de Antioquia, A.A. 1226 Medellín, Colombia.
[b] Grupo de Biofísica, Instituto de Física, Universidad de Antioquia, A.A. 1226 Medellín, Colombia.
[c] Grupo de Estado Sólido-GES, Universidad de Antioquia, A.A. 1226 Instituto de Física, Medellín, Colombia.
[d] Univ. Lille, CNRS, INRAE, Centrale Lille, UMR 8207 - UMET - Unité Matériaux et Transformations, F-59000 Lille, France.

Abstract

Classical Buckingham potentials are used to obtain information on how physical quantities change under lattice and pressure variations at zero temperature in zinc ferrites $(\mathrm{Zn}^{2+}_{1-x}\mathrm{Fe}^{3+}_{x})[\mathrm{Zn}^{2+}_{x}\ \mathrm{Fe}^{3+}_{2-x}]\mathrm{O}_4$. Elastic constants, sound velocities and Debye's temperature, θ_D, are obtained numerically and compared to literature. The potentials predict pressure vs lattice dependencies in agreement with experiments. Additionally, sound velocities along the [100], [110] and [111] crystallographic directions are compared to those in the polycrystalline counterparts to evaluate the anisotropy as a function of pressure. The fastest propagation is predicted along [111] direction and the lowest one along [100], in agreement with experiments. The transverse velocities are predicted asymmetric with respect to the zero-pressure point where they have a maximum and under compression they remain almost constant. In contrast, the longitudinal velocities increase almost linearly under compression. Both transverse and longitudinal velocities decrease quadratically under expansion. Thus, the average sound velocity in the polycrystalline and therefore θ_D, which depends on it, have similar trends. The spinel structure is also investigated as function of the inversion parameter x to address the effect of crystallographic inversion upon sound waves propagation. The average sound velocity and θ_D are barely affected by x as their biggest changes are $\sim$1.9% and $\sim$1.4% respectively, with respect to a normal spinel. Besides, it is found that fluctuations due to ion randomness of octahedral/tetrahedral sites at each fixed x have a smaller role, therefore they can be neglected.

1 INTRODUCTION

Zinc-ferrite $ZnFe_2O_4$ (ZFO), also known as franklinite mineral, has several technological applications: antennas, nanowires, hydrogen storing, power inductors, spintronic devices, soft magnets, electromagnetic interference filters, film transformers in integrated circuits, solar hydrogen production by releasing oxygen from water, etc. [1,2,3,4,5,6,7]. Knowledge of sound waves in ZFO as a function of the lattice parameter and pressure is of relevant importance for many technological applications. For instance, a recent study has shown the existence of a shock wave-induced switchable magnetic phase transition in ZFO ferrite nanoparticles, opening the door to applications of these materials for magnetic sensors [8]. Besides, correlation between structural changes and electrical transport properties have been recently studied experimentally, where pressure-driven dielectric properties have been measured and confirmed that, under pressure, the electrochemical stability of the sample is improved [9]. Moreover, the superparamagnetism of ZFO nanoparticles has been observed under high pressure up to 40 GPa [9], and sound velocities play a relevant role.

Experimentally, sound velocities along different crystallographic directions can be measured by means of the Fisher and McSkimin phase comparison method, and by inversion of the velocity wave equations, the elastic constants C_{11}, C_{12} and C_{44} can be obtained [10]. Thus, several experimental works related to high pressure in normal ZFO spinels have been reported in literature [11,12,13]. For instance, by using high-pressure synchrotron X-ray diffraction with diamond anvil cells, Levy et al. [11] reported results up to 36.6 GPa and a bulk modulus of 166.4(3) GPa. Later, Greenberg et al. [12] warned about the existence of great discrepancies between studies on spinels with the same composition. In that work, authors using He and Ne atmospheres as pressure media in diamond anvil cells, were able to provide controllable quasi-hydrostatic conditions, resulting in a high-quality fit to both second- and third-order equations of state, so they could report pressures in ZFO up to 26 GPa and a bulk modulus of 174(2) GPa. Also Wang et al. [13] studied pressure induced phase transformation by Raman spectroscopy up to 61.9 GPa, finding that ZFO transforms to an orthorhombic structure phase ($CaFe_2O_4$-polymorph) at a pressure of 24.6 GPa or higher. To support these extensive experimental works,

a better atomic theoretical understanding of elastic properties and sound waves in ZFO as a function of pressure is clearly needed. In particular, high-pressure theoretical studies of ZFO mechanical properties as energies, elastic constants, sound waves, Debye's temperature etc. are of relevant importance.

As to our knowledge, there are no molecular dynamics (MD) studies of ZFO sound waves as a function of lattice parameter or pressure, in part due to the lack of potentials describing ZFO systems. Such shortcoming is addressed in this work by studying ZFO spinel structures at 0 K. We first obtain the elastic constants computationally and then the sound waves at zero pressure and zero temperature for normal and inverse phases. After, we vary the lattice parameter to compute the elastic constants. Then, other derived properties such as pressure, bulk moduli, sound waves and Debye's temperature are computed.

2 METHODOLOGY

2.1 Force-field

ZFO Spinel interactions are handled via a Buckingham potential

$$V(r_{ij}) = \frac{z_i z_j e^2}{4\pi\epsilon_0 r_{ij}} + A_{ij}\exp\left(\frac{-r_{ij}}{\rho_{ij}}\right) - \frac{C_{ij}}{r_{ij}^6}, \quad (1)$$

where z_i and z_j are the charges of two ions separated a distance r_{ij}, and A_{ij} ρ_{ij}, C_{ij} are fitting parameters. In previous works, the Zn-O pair potential has been tested to observe the response of zinc oxide nanobelts under tensile loading [14,15], while the Fe-O potential has been used to simulate some magnetite properties like diffusion [16], so that combined they can reproduce most of the structural ZFO properties. For cation interactions, Fe-Fe, Zn-Zn and Zn-Fe, only the Coulomb term is included. Parameters employed are displayed in **Table 1**.

Table 1. Buckingham spinel parameters for ZFO spinel systems [14,15,16].

Pair	z_i	z_i	A_{ij}(eV)	ρ_{ij}(Å)	C_{ij}(eVÅ^6)
$Zn^{2+}O^{2-}$	+2	-2	529.70	0.3581	0
$Fe^{3+}O^{2-}$	+3	-2	1414.6	0.3128	0
$O^{2-}O^{2-}$	-2	-2	9547.96	0.2192	32
FeFe, ZnZn, ZnFe (only Coulomb term used)					

The Buckingham potential is a long-range interaction potential which is handled through Ewald summation [17], which requires setting a cut-off distance r_c for computing long-range interactions into the *k*-space, a desired relative error ϵ in forces and a damping parameter α (chosen as the predefined value computed by LAMMPS at the defined precision but guaranteeing full relaxation). Contrary the finite temperature simulations, in minimizations, the coulombic part can be cumbersome since the procedure may stop if the algorithm is not able to reduce the energy. That is, from one step to the next, the code stops if the change in energy is lower than the machine precision although the force is not yet zero, leading to incorrect values of the elastic constants. The trick is to choose the parameters so that the Ewald sums converge rapidly but avoiding the problems of no full minimization. In this work, the cut-off distance was set to $r_c = 16$ Å and the precision was set to $\epsilon = 10^{-10}$, which is much smaller than the usual values of around $\sim 10^{-4}$ reported for MD simulations at finite temperature [16].

2.2 Elastic constants and their related properties

We follow the standard static procedure to obtain the elastic constants through discrete deformations of the box followed by fixed-volume energy minimization (see, for example, Ref. [18,19]). In a spinel, and in agreement with experiments [10,20,21,22,23], Buckingham potentials predict symmetrical spinel structures where the components C_{11}, C_{12}, C_{44} are the only elastic constants different from zero. They are used to compute the polycrystalline bulk modulus B and shear modulus G, following the Voigt-Reuss-Hill scheme [24,25],

$$B = \frac{C_{11} + 2C_{12}}{3}, \tag{2}$$

$$\begin{aligned} G &= \frac{G_R + G_V}{2}, \\ G_V &= \frac{(C_{11} - C_{12}) + 3C_{44}}{5}, \\ G_R &= \frac{5(C_{11} - C_{12})C_{44}}{3(C_{11} - C_{12}) + 4C_{44}}. \end{aligned} \tag{3}$$

Because some fundamental properties are related to the directional sound wave velocities, it is also useful to compute propagation of these velocities for a single crystal spinel. Therefore, velocities propagation of the sound waves in the crystallographic directions [100], [110] and [111] are calculated using the relations obtained from the Christoffel equations [26,27]

$$\begin{aligned} v_{L[100]} &= \sqrt{C_{11}/\rho}, \\ v_{T[100]} &= \sqrt{C_{44}/\rho}, \\ v_{L[110]} &= \sqrt{(C_{11} + C_{12} + 2C_{44})/2\rho}, \\ v_{T1[110]} &= \sqrt{C_{44}/\rho}, \\ v_{T2[110]} &= \sqrt{(C_{11} - C_{12})/2\rho}, \\ v_{L[111]} &= \sqrt{(C_{11} + 2C_{12} + 4C_{44})/3\rho}, \\ v_{T[111]} &= \sqrt{(C_{11} - C_{12} + C_{44})/3\rho}, \end{aligned} \tag{4}$$

where L and T stand for longitudinal and transverse polarizations of the acoustic waves respectively. Usually, experimentalists use these velocities and by inversion of three of them (e.g., equations along [110]), obtain the elastic constants C_{11}, C_{12} and C_{44}[10]. They are also related to the mean peaks in the infrared spectrum [28]. According to Anderson [29], the sound velocity in a polycrystalline system can be approximated as the average sound velocity over all possible lattice orientations of a single crystal as B and G moduli for the aggregate invariably lie between the Reuss and Voigt values [24], so

$$v_m = \left(\frac{1}{3}\left[\frac{2}{v_s^3} + \frac{1}{v_l^3}\right]\right)^{-\frac{1}{3}}, \quad (5)$$
$$v_s = \sqrt{\mathrm{G}/\rho},$$
$$v_l = \sqrt{\frac{B + \frac{4G}{3}}{\rho}},$$

where v_l and v_s are the longitudinal and shear (transverse) elastic sound velocities. Thus, following the Anderson discussion [29], here we approximate the polycrystalline by considering this average over calculations on a single crystal rather than creating a bit box aggregate. A more realistic approximation to a polycrystalline would be to use a box of an aggregate of crystals (sample formed of many grains), nevertheless, Anderson showed that his approximation fits well to experiments. Compared to previous sound waves, it provides a consistent measure of how the acoustic properties of the material deviate from isotropy. Anderson also showed that v_m can be used to approximate the Debye's temperature

$$\theta_D = \frac{h}{k_B}\left(\frac{3nN_a\rho}{4\pi M}\right)^{1/3} v_m = \frac{h}{k_B}\left(\frac{3n}{4\pi}\right)^{1/3}\frac{v_m}{a}, \quad (6)$$

where $h/k_B = 4.7992431 \times 10^{-11}$ K·s, is the ratio of the Planck and Boltzmann constants, $n = 56$ is the number of ions in the spinel, N_a is Avogadro's number, $\rho = M/N_a a^3$ is the density, $M = mN_a$ is the molecular weight, a is the lattice parameter and $m = 1928.528$ u is the total mass of the unit cell. Therefore, for computations we can use the fact that in cubic systems $\theta_D(a) \propto v_m(a)/a$.

2.3 Samples used

In general, the ZFO belongs to the space group Fd$\bar{3}$m, no. 227. Thus, its unit cell consists of 56 ions organized in a face centered cubic (fcc) structure, of which 32 are O^{2-} anions and, Zn, Fe cations occupy 8 tetrahedral and 16 octahedral sites respectively. The general stoichiometric formula for a ZFO spinel is $(\mathrm{Zn}_{1-x}^{2+}\mathrm{Fe}_x^{3+})[\mathrm{Zn}_x^{2+}\ \mathrm{Fe}_{2-x}^{3+}]\mathrm{O}_4$, where () and [] stands for tetrahedral and octahedral sites respectively [30,31]. The parameter x is known as the inversion degree and

has the value $x = 0$ for a normal spinel being the most common found experimentally, whereas $0 < x < 1$ represents a partial-inverse ZFO spinel.

In our simulations, for a normal spinel, a single unit cell with 56 ions was considered, whereas for the partial-inverse spinels, a box of 3×3×3 units cells was used for all minimizations. These sizes were enough to account for the effects considered here. Partial inverse spinels were constructed by shuffling ions with the Fisher-Yates algorithm [32]. For each value of x, 400 runs (differing by ion shuffling) were performed to account for the fluctuations due to randomization of Zn and Fe ions at tetrahedral and octahedral sites.

3 RESULTS AND DISCUSSION

Using a standard minimization procedure at zero-pressure we have computed the lattice parameter, the elastic constants, the bulk modulus B, the shear modulus G, and the Debye's temperature θ_D for the normal and partial inverse spinels, as given by relations (2) to (3). The results are summarized in **Table 2** and compared to experimental data found in literature [10,21,22,23].

Experimental data for elastic constants of a ZFO-normal spinel vary greatly as shown in **Table 2**. Our computations are closer to the experimental results reported by Lewis and Catlow [21], with differences of ∼27%, ∼4% and ∼11% for C_{11}, C_{12} and C_{44} respectively (computed as $\frac{|C_{Buck} - C_{expt}|}{|C_{expt}|} 100$), and also similar to their MD study using a Shell-model potential, while a comparison to experiments of Li et al [10], gives differences of 32%, ∼1.2% and ∼46%. Two samples of an inverse and a partial inverse spinels are also given in **Table 2** where it is observed similar results to that of a normal spinel. However, compared to more resent ultrasound velocity measurements (performed on a high-purity ZFO single crystal, grown by the flux method) by Watanabe et al. [33] the discrepancies with our data are larger, e.g., ∼80% for C_{44}. Their measurements are in better agreement with the DFT predictions than with our MD results.

On the other hand, the cation random mixing in tetrahedral and octahedral sites does not affect the lattice parameter and bulk moduli significantly.

Table 2. Lattice constant a_0(Å), bulk modulus B(GPa), shear modulus G(GPa), elastic constants (GPa). Standard deviations over 400 samples are given for inverse (x=1) and partial inverse spinels ($x = 0.5$). Underlined θ_D(K) are computed from elastic constants (we assume $a_0 = 8.441$ Å to get density when lattice is not given by authors).

ZFO-Spinel	a_0	B	G	C_{11}	C_{12}	C_{44}	θ_D
Normal (x=0.0)	8.479	212.8	119.4	338.0	150.2	140.2	712.1
Inverse (x=0.5)	8.445	208.6	113.4	316.1	155.1	142.7	693.3
	± 0.013	± 1.1	± 0.6	± 2.7	± 0.8	± 0.8	± 2.4
Inverse (x=1.0)	8.391	230.5	115.5	331.7	179.9	153.0	698.6
	± 0.008	± 0.6	± 0.5	± 2.3	± 0.5	± 0.7	±1.9
Other works							
DFT (Meng[20])	8.52	170.30	59.10	219.20	145.84	81.36	507.4
MD (Lewis[21])	--	203.3	114.2	322	144	131	689.1
Expt (Lewis[21])	--	193.0	115.8	265	157	157	659.0
Expt (Grimes[22])	--	193.0	93.49	265	157	135	630.9
Expt (Li [10])	8.441	182.4	74.6	250.5	148.4	96.2	565.6
Expt (Gholizadeh[23])	8.5	77.7	49.91	144.3	44.42	48.09	454.7
Expt (Watanabe[33])	--	171.5	62.5	233.8	140.8	75.9	518.8

Our equilibrium θ_D value for a normal ZFO-spinel of 712 K is higher compared with the experimental value of ~555 K predicted by infrared spectroscopy [34,35] (Experimentally, there are several ways to compute θ_D [36]: one is from the average of the root mean square of the four infrared temperatures obtained from the main frequencies , $\nu_1 = 555$ cm^{-1}, $\nu_2 = 393$ cm^{-1}, $\nu_3 = 325$ cm^{-1}, $\nu_4 = 169$ cm^{-1}, by using the formula $\theta_i = hc\nu_i/k_B = 1.438\nu_i$, which gives $\theta_D = 555$ K). Our computational prediction of θ_D is similar to the one predicted experimentally of 659 K [30], and also by MD using Lewis' potential of 689 K [21]. Our large value of θ_D is due to the fact that our predicted elastic constants are greater than the experimental ones, so the average sound velocity is also bigger in our computations, increasing our θ_D estimation. In contrast, DFT simulations of Meng et al. reported a smaller prediction, namely 507.4 K [20]. Experimental results reported by Gholizadeh [23] for nanoparticles —in contrast to a bulk system— are very different to ours and to the DFT and experiments reported by Lewis or Li [10,20,21]. Gholizadeh reported $\theta_D = 487.5$ K, however, we found a value of 454.7 K using their reported elastic constants (Gholizadeh uses the same formula (6) to get θ_D but takes $v_l = v_{L[100]}$ and $v_s = v_{T[100]}$).

The average sound velocities for a polycrystalline (expressions (5)) as well as the acoustic wave velocities propagating along the [100], [110] and [111] crystallographic directions for a single crystal (expressions (4)) are summarized in **Table 3**. Our results are also compared to other velocities computed from elastic constants reported in the literature [10,20,21,23]. In general, there are noticeable differences between different authors. Watanabe et al., in ref. [33], report $v_{L[100]} \approx 6620$ m/s, $v_{T2[110]} \approx 2960$ m/s, and $v_{T1[110]} \approx 3770$ m/s at 0 K, however, they do not mention the density and lattice used, so for computations of **Table 2** and **Table 3** we have used a lattice of 8.441 Å. Interestingly, they also show that these velocities do not vary much with temperature up to 300 K. For example, these velocities at 0 K differ from the measured sound velocities at 300 K by ~2%, ~1%, and ~0.8%, respectively. In fact, the MD errors are larger, so temperature effects can be ignored in our MD calculations.

Our prediction of the sound velocity v_m is larger compared to experiments, however it is similar to the Lewis' MD calculations [21]. We see in **Table 3** that for each row, when comparing v_l and v_s of a polycrystal (isotropic), for each direction of a single crystal (anisotropic), the longitudinal velocities are similar to v_l and analogously when comparing v_s to all transversal velocities. This indicates the degree of anisotropy along every single direction with respect to the average. Comparing experimental data in **Table 2** and **Table 3**, reveals some differences which could depend on several factors, e.g., synthesis conditions used. DFT underestimates values as B or v_m but Buckingham overestimates them.

Table 3. Average sound velocities [m/s] (polycrystalline) and acoustic wave velocities [m/s] propagating along the [100], [110] and [111] crystallographic directions (single crystal) in a normal ZFO-spinel. All data are computed from elastic constants reported in the respective references.

	v_m	v_l	v_s	$v_{L[100]}$	$v_{T[100]}$	$v_{L[110]}$	$v_{T1[110]}$	$v_{T2[110]}$	$v_{L[111]}$	$v_{T[111]}$
Buck-ZFO	5301	8415	4767	8021	5166	8553	5166	4228	8723	4562
DFT (Meng[20])	3795	6936	3378	6506	3964	7139	3964	2662	7337	3156
MD (Lewis[21])	5106	8141	4590	7776	4960	8268	4960	4088	8426	4398
Expt (Lewis[21])	4883	7867	4386	7055	5430	8313	5430	3185	8693	4073
Expt (Grimes[22])	4675	7724	4190	7055	5035	8061	5035	3185	8370	3900
Expt (Li [10])	4192	7276	3743	6859	4251	7451	4251	3096	7639	3523
Expt(Gholizadeh[23])	3393	5233	3060	5260	3037	5227	3037	3095	5215	3076
Expt(Watanabe[33])	3845	6918	3425	6626	3776	7028	3776	2962	7157	3256

In contrast to a normal spinel, we did not find reported experimental data of elastic constants in partial-inverse spinels. Partial-inverse spinel formation depends on the synthesis

conditions and there is not, so far, any standard procedure to control the value of the inversion parameter for their fabrication as a function of inversion parameter x; this is still an active and open research field. For this reason we get them computationally, and data were used to get average sound velocities and θ_D versus x (averages over 400 random samples for each value of x). Results are shown in **Figure 1**. In general, it is observed a quadratic behavior as a function of x. Although the change of θ_D and the average velocities in a polycrystal are not as large as when the lattice parameter varies, we observe that the partial inverse spinel with $x \sim 0.6$ has the biggest change of $\sim$ 1.4% respect to the normal spinel. Similarly, for the sound velocity, the change is around $\sim$ 1.9%. We also observe that while longitudinal velocity v_l is larger for inverse spinel, the shear velocity v_s is lower than in the normal spinel.

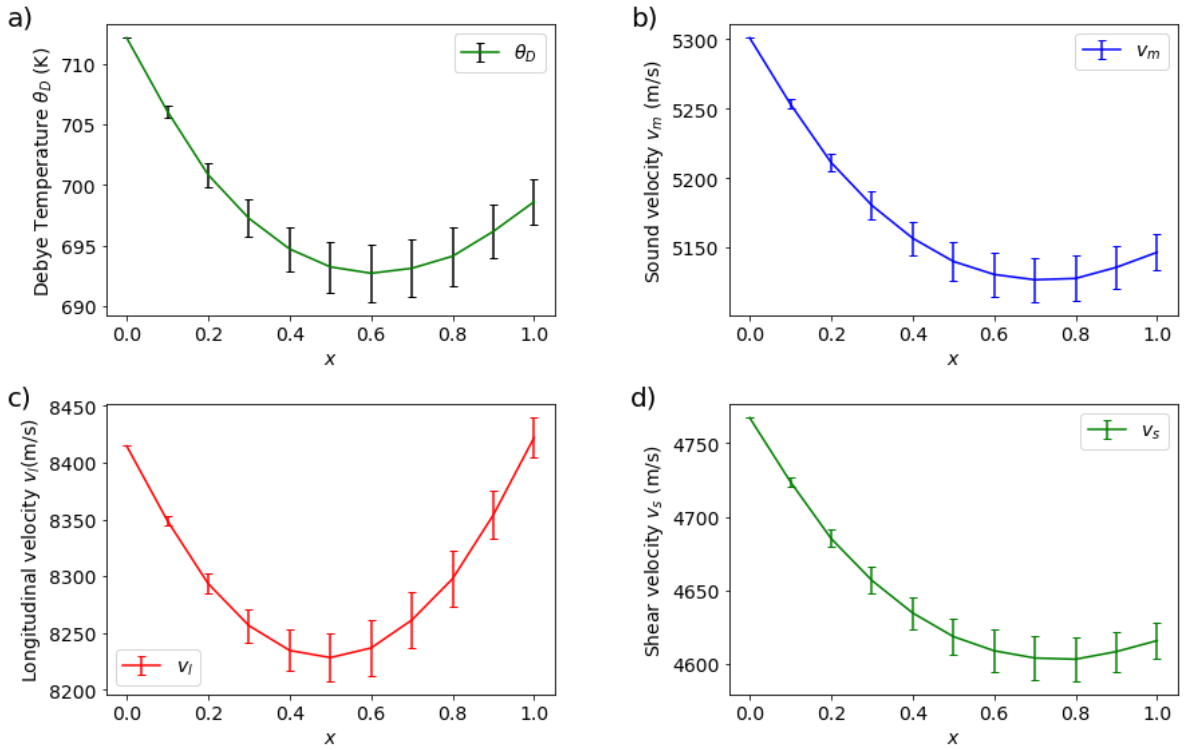

Figure 1. a) Debye's temperature θ_D, b) average sound velocity, c) the longitudinal and d) shear (transverse) elastic sound velocities as function of the inverse parameter, x for $(Zn^{2+}_{1-x}Fe^{3+}_{x})[Zn^{2+}_{x}\ Fe^{3+}_{2-x}]O_4$ spinel.

In the following we study the physical properties of a ZFO normal spinel as a function of pressure. Pressure and minimum energies are compared to the Murnaghan equation of state where energy is written as a function of lattice parameter [37],

$$E(a) = E_0 - \frac{B_0 a_0^3}{B_0' - 1} + \frac{B_0 a^3}{B_0'}\left[\frac{(a_0/a)^{3B_0'}}{B_0' - 1} + 1\right], \tag{7}$$

here, B' is the experimentally found derivative of the bulk modulus B with respect to pressure $P = -dE/dV$. The variation is done in the interval 8.0 Å to 9.0 Å, which represents a change of approximately ~6% in the strain (beyond these limits the spinel structure is destroyed). The respective plots are given in **Figure 2**a). Negative pressure results are included in our calculations to unveil the asymmetry respect to the strain and lattice parameter. Minimum energies for a normal and inverse spinel are also plotted in **Figure 2**b) and compared to the Murnaghan equations of energy. Our predictions are more in agreement with results of Greenberg et al. [12] than with results of Levy et al. [11]. According to these experimental works, a phase transition it is observed at pressures of ~25 GPa, but this transition is predicted by the Buckingham potential around ~50 GPa ($a < 8$ Å). There are also discrepancies between the Buckingham results and the Birch-Murnaghan equation at positive pressures. This could be due to the fact that the experimental samples are sintered from powder whereas we have considered a perfect bulk crystal in MD. However, at positive pressures, Buckingham's predictions are in agreement up to ~25 GPa; before the transition phase around ~8.17 Å. Obviously, interaction forces in either a compressed powder or a sintered polycrystalline bulk, are different to interactions in a perfect single crystal because of the discontinuities and defects at grain boundaries. So, grain boundaries increase the energy and reduce the bulk modulus. Based on this and on the error bars, we guess here that the potential does work for positive pressures applied to a perfect bulk crystal.

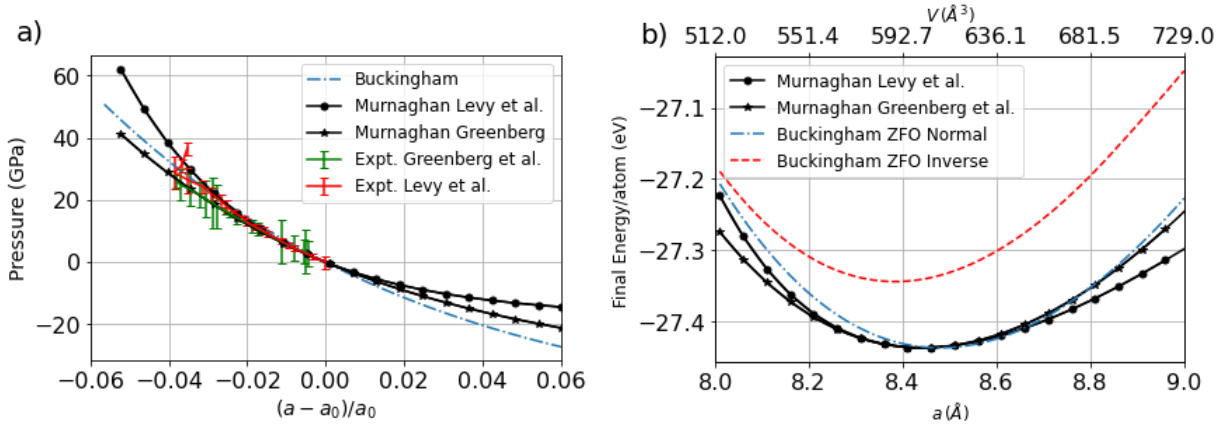

Figure 2. a) Pressure vs strain in a normal spinel. In red, experimental data of Levy et al. [11] and in green, data of Greenberg et al. [12]. In black, Murnaghan equation of state using experimental values of Levy: $B = 166.4$ GPa,

$B' = 9.3$ and Greenberg: $B = 174.4$ GPa, $B' = 4$. b) final energies/ion after minimization, in top, volume V. In blue dashed-dotted line, Buckingham energy of a normal spinel and in red dashed line, comparison to an inverse spinel.

It is also interesting to see how the lattice compression or expansion affects the velocity propagation of the sound waves in a single crystal system; the plots are shown in **Figure 3**. The change of pressure as a function of the lattice parameter is given on the top axis. In general, the transversal velocities $v_{T[hkl]}$ reduce with a lattice expansion and increase under compression, whereas the longitudinal velocities $v_{L[hkl]}$ are asymmetric curves with maxima around zero-pressure. In **Figure 3**d) we also show the respective elastic constants computed numerically (analytical deductions of the elastic constants for an ideal spinel are indeed found in literature but formulations are restricted to the harmonic theory [38,39,40]). We observe that $(C_{11} - C_{12})$ and C_{44} have similar trends and in contrast to C_{11} they do not exhibit significant changes. That explains why $v_{T2[110]}$ does not vary too much in the interval whereas $v_{T1[110]}$ does change proportionally to the root of the C_{44}; similar analyses can be done for the other directions. Along direction [100], the transversal velocity is dominant whereas along directions [110] and [111] is the longitudinal term. The fastest propagation is along [111] direction and the lowest along [100]. Both of them increase linearly with positive pressure, but they decrease quadratically under negative pressure.

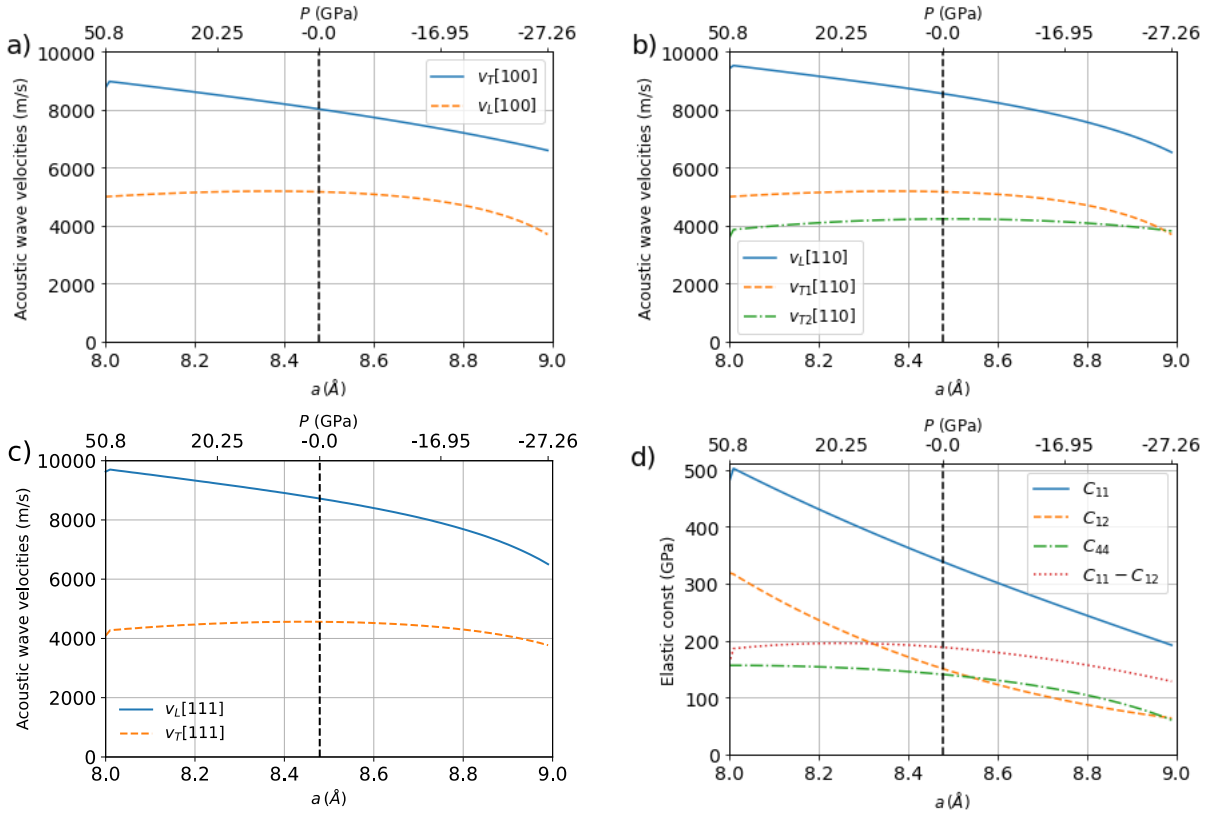

Figure 3. Acoustic wave velocities along the crystallographic directions: a) [100], b) [110], c) [111] and d) the elastic constants for the ZFO normal spinel vs lattice. In top pressure variation.

In the case of a polycrystal we also investigate the variation of the θ_D and the average sound velocities as a function of the lattice parameter. More exactly, in **Figure 4** we show the plots of the θ_D and the respective average sound velocities. We observe that θ_D has a parabolic behavior increasing under sample compression (positive pressure) but decreasing under lattice expansion (negative pressure). Analyzing the average sound velocity v_m and its two components v_l and v_s, we see that v_l gives the largest contribution to θ_D.

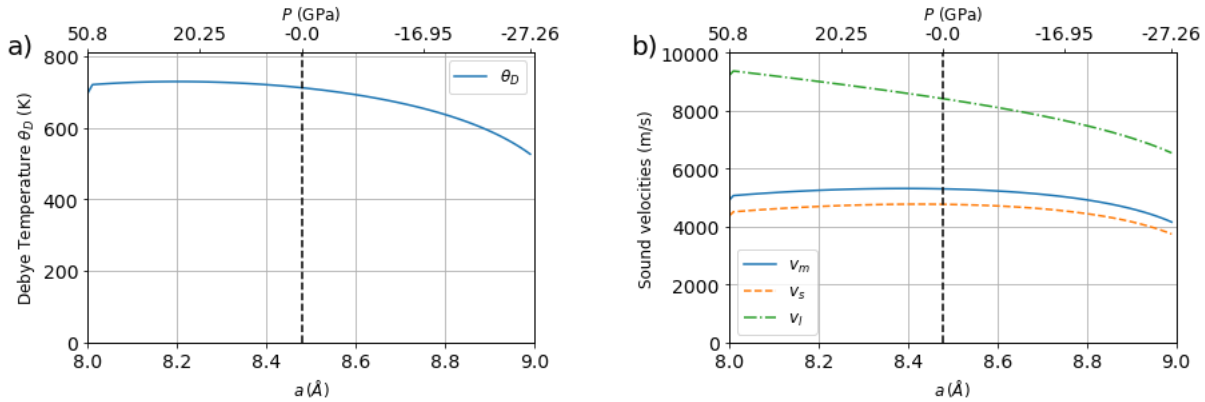

Figure 4 a) Debye's temperature, θ_D, vs lattice parameter a. b) Average sound velocity v_m and v_l, v_s are the longitudinal and shear (transverse) elastic sound velocities for the ZFO normal spinel. In top the pressure P.

To get a better understanding, in **Figure 5**a) we plot the Debye's temperature θ_D versus the change of energy $\Delta E = E_{min}(P) - E_{min}$ and, and in **Figure 5**b) versus pressure P. As we observe, although the lattice compression or expansion produces the same increase in energy (up to a maximum of $\sim$ 0.2 eV), the change in θ_D, is not symmetric, i,e., an expansion produces a variation of $\Delta\theta_D \sim 512$ K whereas a compression produces only a variation of $\Delta\theta_D \sim 17$ K; this is observed in both plots. This feature tells us that a compression does not affect too much the θ_D and so their related quantities.

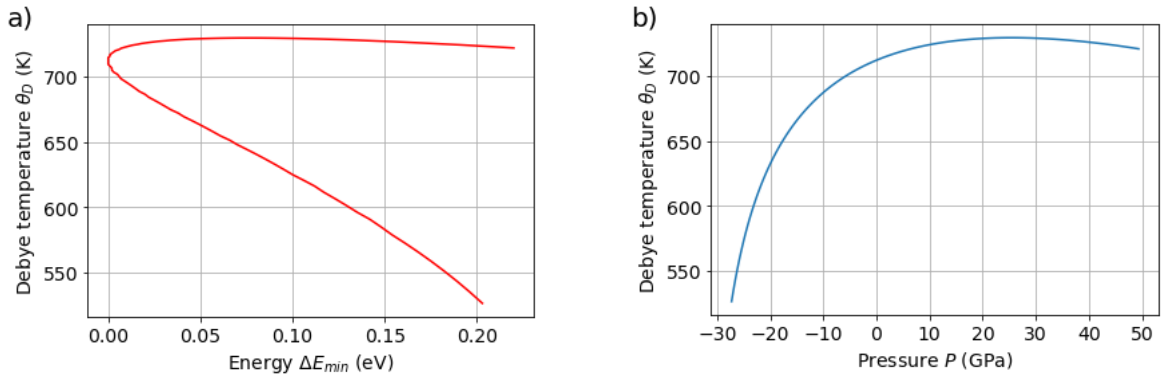

Figure 5. a) Changes of the Debye's temperature, θ_D, vs energy and b) vs pressure as the lattice changes for the ZFO normal spinel. $\Delta E_{min} = E_{min} - E_{min}(P = 0)$.

4 CONCLUSIONS

Using Buckingham potentials, we have investigated the mechanical properties of ZFO spinels. Elastic constants and sound velocities along the [100], [110] and [111] crystallographic directions are compared to average sound velocities in the polycrystalline structure thus getting an insight of the degree of anisotropy. At zero pressure, noticeable differences are found between our predictions and some values found in literature. The potentials predict that transverse velocities are asymmetric with respect to the zero-pressure point where they have the maximum value and that under compression, they do not exhibit significant changes, in contrast to the longitudinal velocities, which vary monotonically with the lattice parameter. This behavior is also reflected in the average sound velocities and thus in Debye's temperature θ_D

which has a direct impact on many physical properties such as self-diffusion, melting point, lattice thermal conductivity, specific heat, entropies, Bragg intensities, electrical resistivity, etc. [41].

Experimentally it is very difficult to investigate spinel structures as a function of the inversion parameter x. Here, this limitation is circumvented by using computational simulations to address the effect of crystallographic inversion upon sound waves propagation. From our simulations we conclude that the inversion parameter does not produce noticeable changes on sound waves, so these changes should be difficult to be noticed experimentally. Nevertheless, the potentials predict that the longitudinal velocity has its minimum value at $x \approx 0.5$, whereas, for the shear velocity, the minimum value is at $x \approx 0.7$. This has an impact on Debye's temperature θ_D, whose lowest value is around $x \approx 0.6$. This could have connection to other properties depending on x, indeed, high saturation magnetization, for instance, is predicted experimentally when $x \approx 0.5$ [7,42]. Moreover, experimentally magnetic moments in structures such as $Ni_{1-x}Zn_xFe_2O_4$, are found to have a maximum around $x \approx 0.6$ [43]. This is not a coincidence, since many of the magnetic changes are associated with structural changes.

Despite some discrepancies with the experimental data, the Buckingham potentials presented here are therefore a useful tool for further investigating the mechanical and structural properties of the ZFO spinels under conditions that cannot be achieved by currently available modelling approaches. However, better potentials are still required.

In summary, this work highlights the utility of Buckingham potentials for the study of sound velocities and Debye's temperature in bulk ZFO spinel systems as a function of lattice parameter a, pressure and inversion parameter x, thus revealing their properties more clearly.

Acknowledgements: We thank Normand Mousseau for computer resources and corrections. This work was supported in part by grants from the Natural Sciences and Engineering Research Council of Canada (NSERC). We are grateful to Calcul Québec/Compute Canada (CQ/CC) for generous allocations of computer resources. O. R. and J. R. acknowledges University of Antioquia for the exclusive dedication program and to the CODI-UdeA 2020-34211, 2022-51311, 2022-51312, and 2022-51330 project for financial support. O. Arnache wants to thank for the financial support by Solid State Group - GES at the University of Antioquia in the framework of Sustainability Strategy 2020-2021, SIIU 2019-26150 project and by Colombian ministry of science

and technology - Minciencias (project no. 111580863381, contract 325-2019 - Acta CODI-2019-25990).

Bibliography

1 Z. Ž. Lazarević, Č. Jovalekić, A. Milutinović, D. Sekulić, V. N. Ivanovski, A. Rečnik, B. Cekić, and N. Ž. Romčević, Journal of Applied Physics **113**, 187221 (2013).
2 K. Shimokawa, T. Atsumi, M. Harada, R. E. Ward, M. Nakayama, Y. Kumagai, F. Oba, N. L. Okamoto, K. Kanamura, and T. Ichitsubo, J. Mater. Chem. A **7**, 12225 (2019).
3 M. Goodarz Naseri, E. B. Saion, and A. Kamali, ISRN Nanotechnology **2012**, 1 (2012).
4 M. Virumbrales, R. Sáez-Puche, V. Blanco-Gutiérrez, and M. J. Torralvo-Fernández, J. Phys. Chem. C **121**, 4029 (2017).
5 Y.-C. Liang and H.-Y. Hsia, Nanoscale Res Lett **8**, 537 (2013).
6 Y. Tamaura and H. Kaneko, Solar Energy 78, 616 (2005).
7 J. Wu, N. Li, J. Xu, Y. Jiang, Z.-G. Ye, Z. Xie, and L. Zheng, Appl. Phys. Lett. **99**, 202505 (2011).
8 V. Mowlika, A. Sivakumar, S. A. Martin Britto Dhas, C. S. Naveen, A. R. Phani, and R. Robert, J Nanostruct Chem **10**, 203 (2020).
9 J. Zhang, Y. Zhang, X. Wu, Y. Ma, S.-Y. Chien, R. Guan, D. Zhang, B. Yang, B. Yan, and J. Yang, ACS Appl. Mater. Interfaces **10**, 42856 (2018).
10 Z. Li, E. Fisher, J. Liu, M. V. Nevitt. J Mater Sci. **26**, (1991) 2621–4.
11 D. Levy, A. Pavese, and M. Hanfland, Phys Chem Min **27**, 638 (2000).
12 E. Greenberg, G. Kh. Rozenberg, W. Xu, R. Arielly, M. P. Pasternak, A. Melchior, G. Garbarino, and L. S. Dubrovinsky, High Pressure Research **29**, 764 (2009).
13 Z. Wang, D. Schiferl, Y. Zhao, and H. St. C. O'Neill, Journal of Physics and Chemistry of Solids **64**, 2517 (2003).
14 Binks DJ. *Computational Modeling of Zinc Oxide and Related Oxide Ceramics*. Department of Chemistry, University of Surrey, Harwell, England, 1994.
15 A. J. Kulkarni, M. Zhou, and F. J. Ke, Nanotechnology **16**, 2749 (2005).
16 J. Vaari, Solid State Ionics **270**, 10 (2015).
17 C. J. Fennell and J. D. Gezelter, The Journal of Chemical Physics **124**, 234104 (2006).
18 S. Plimpton, Journal of Computational Physics **117**, 1 (1995).
19 Ó. A. Restrepo, Ó. Arnache, J. Restrepo, C. S. Becquart, and N. Mousseau, Computational Materials Science **213**, 111653 (2022).
20 Y. Meng et al. Materials Science and Engineering 569 (2019) 022016.
21 G. V. Lewis and C. R. A. Catlow, J. Phys. C: Solid State Phys. **18**, 1149 (1985).
22 N. W. Grimes, Physica Status Solidi (b) **58**, K129 (1973).
23 A. Gholizadeh, J. Nanoanalysis., 5, (2018) 7-16.
24 R. Hill, Proc. Phys. Soc. A **65**, 349 (1952).
25 M. Jamal, S. Jalali Asadabadi, I. Ahmad, and H. A. Rahnamaye Aliabad, Computational Materials Science **95**, 592 (2014).

26 C. Kittel, *Introduction to Solid State Physics*, 8th ed (Wiley, Hoboken, NJ, 2005), page 83.
27 A. K. Kushwaha, R. Khenata, A. Bouhemadou, S. Akbudak, and R. Ahmed, Bull Mater Sci **43**, 263 (2020).
28 N. W. Grimes, Spectrochimica Acta Part A: Molecular Spectroscopy **28**, 2217 (1972).
29 O. L. Anderson, Journal of Physics and Chemistry of Solids **24**, 909 (1963).
30 K. E. Sickafus, J. M. Wills, and N. W. Grimes, Journal of the American Ceramic Society **82**, 3279 (2004).
31 C. Yao, Q. Zeng, G. F. Goya, T. Torres, J. Liu, H. Wu, M. Ge, Y. Zeng, Y. Wang, and J. Z. Jiang, J. Phys. Chem. C **111**, 12274 (2007).
32 R. A. Fisher and F. Yates, *Statistical Tables for Biological, Agricultural and Medical Research* (Oliver and Boyd, London, 1948), page 26.
33 T. Watanabe, S. Takita, K. Tomiyasu, and K. Kamazawa, Phys. Rev. B **92**, 174420 (2015).
34 N. W. Grimes, Philosophical Magazine **25**, 67 (1972).
35 S. E. Ziemniak, L. M. Anovitz, R. A. Castelli, and W. D. Porter, Journal of Physics and Chemistry of Solids **68**, 10 (2007).
36 F. H. Herbstein, Advances in Physics **10**, 313 (1961).
37 F. D. Murnaghan, Proc Natl Acad Sci USA **30**, 244 (1944).
38 M. E. Striefler and G. R. Barsch, Journal of Physics and Chemistry of Solids **33**, 2229 (1972).
39 C. Sammis, Geophysical Journal International **29**, 15 (1972).
40 C. G. Sammis, Geophysical Journal International **19**, 285 (1970).
41 H. M. Ledbetter and R. P. Reed, Journal of Physical and Chemical Reference Data **2**, 531 (1973).
42 A. Milutinović, Z. Lazarević, Č. Jovalekić, I. Kuryliszyn-Kudelska, M. Romčević, S. Kostić, and N. Romčević, Materials Research Bulletin **48**, 4759 (2013).
43 G. D. Tang, D. H. Ji, Y. X. Yao, S. P. Liu, Z. Z. Li, W. H. Qi, Q. J. Han, X. Hou, and D. L. Hou, Appl. Phys. Lett. **98**, 072511 (2011).